Contents lists available at ScienceDirect

Materials Today Physics

Zn: a versatile resonant dopant for SnTe thermoelectrics

D.K. Bhat [a, *], U.S. Shenoy [b, **]

[a] Department of Chemistry, National Institute of Technology Karnataka, Surathkal, Mangalore - 575025, India
[b] Department of Chemistry, College of Engineering and Technology, Srinivas University, Mukka, Mangalore - 574146, India

ARTICLE INFO

ABSTRACT

SnTe-based materials have been receiving increasing heed in the field of thermoelectrics (TEs) because of their tunable electronic structure. Until now, only In and Bi are reported to introduce resonance level in SnTe. In this work, for the very first time, we report Zn as a resonant dopant in SnTe using first-principles density functional theory calculations. We show that the resonant states introduced by Zn raises the heavy hole valence sub-band above light hole valence sub-band leading to both record high room temperature Seebeck coefficient ($\sim$127 μVK^{-1} at 300 K) and figure of merit, ZT ($\sim$0.28 at 300 K) for SnTe-based materials. The transport properties calculated using Boltzmann transport equations predicts Zn-doped SnTe to be a promising TE material, further confirmed by experimental $ZT_{maximum}$ of $\sim$1.49 at 840 K and $ZT_{average}$ of $\sim$0.78 with 300 K and 840 K as cold and hot ends, respectively.

1. Introduction

Thermoelectric (TE) materials are considered as Holy Grail for the remedial measure of energy and environmental crisis. The dimensionless figure of merit, ZT, which governs the effectiveness of TE material, is given by equation (1).

$$ZT = \frac{\sigma S^2}{\kappa_e + \kappa_L} T \qquad (1)$$

where 'σ' is the electrical conductivity, 'S' is the Seebeck coefficient, 'σS^2' is called the power factor, 'κ_e' is the electronic thermal conductivity, 'κ_L' is the lattice thermal conductivity, 'T' is the absolute temperature, and 'Z' stands for Zahl (German word for number/figure). Although the terms 'σ', 'S', and 'κ_e' are interdependent via the carrier concentration 'N_p', 'κ_L' is the only term which can be tuned independently [1]. Several techniques such as introduction of atomic point defects, nanostructuring, mesostructuring, all-scale hierarchical architecturing and strain engineering have been implemented to reduce κ_L [2–4]. The power factor of the TE materials has been improved by (i) optimizing the carrier concentration by addition of donor dopant or self compensation; (ii) improving the Seebeck values by resonant doping or increase of valley degeneracy by band convergence; (iii) reducing the bipolar effect by increasing the band gap by elemental doping [5–7]. In spite of the advancements in various techniques for improving ZT, the quest for development of environmentally friendly cost-effective TE materials is ever increasing.

Lead-free SnTe has been gaining tremendous interest recently as a potential TE material for the reversible conversion of temperature difference into electrical potential [6,7]. Although SnTe has low ZT because of its inherent vacancies and not so beneficial electronic structure, it can be engineered by means of doping [6,7]. In doping in SnTe is known to introduce resonance level and cause valence band convergence whereas Bi tunes the carrier concentration apart from acting as a resonant dopant [3,8–10]. Ag, Ca, Cd, Hg, Mg, and Mn doping is implemented to increase the bandgap of the material and make the valence band converge [11–16]. Co/multielement doping has been used to introduce various beneficial effects of the added dopants simultaneously into SnTe [17–24]. Codopant selection and concentration optimization to achieve higher power factor is tricky as dopants such as In can drastically reduce the electrical conductivity at higher concentration and dopants such as Ag, Ca, and Mn are not effective in increasing the bandgap of the material when codoped with In whereas Cd and Hg are toxic in nature [18–21]. In addition, solubility of the dopants in SnTe is another bottle neck issue, making the problem still worse [13]. The existing resonant dopants viz. In and Bi have only mediocre ZT of around 1.1 at 873 K

* Corresponding author.
** Corresponding author.
E-mail addresses: denthajekb@gmail.com (D.K. Bhat), sandhyashenoy347@gmail.com (U.S. Shenoy).

[8,9]. Furthermore, *Mn-Cu-Ge* multidoped SnTe, which by far holds the highest ZT of ~1.8, has a power factor of only ~19 $\mu Wcm^{-1}K^{-2}$ at 900 K despite the reduction in valence band offset and introduction of interstitials through multidoping process [17]. This indicates that there is a need to develop strategies to enhance the power factor although simultaneously keeping the thermal component low. Therefore, a search for a non-toxic, cost-effective resonant dopant for SnTe, which can introduce as many beneficial properties as possible is very much relevant and indeed a need of the day.

In this work, we studied the effect of *Zn* on the electronic structure of SnTe at various concentrations using first principles density functional theory (DFT). As theoretical calculation of the transport properties using Boltzmann transport equations predicted *Zn*-doped SnTe to be a potential TE material, we also carried out experimental studies. We prepared *Zn*-doped SnTe using self-propagating high-temperature synthesis (SHS) followed by direct current sintering (DCS) and studied its TE properties. For the first time, we report that a single dopant viz. *Zn* has the ability to introduce various favorable properties into SnTe making it a promising TE material.

2. Results and discussion

We carried out electronic structure calculations of SnTe and *Zn*-doped SnTe using supercells of different sizes to mimic various concentrations. The electronic structure of pristine SnTe ($Sn_{32}Te_{32}$) reveals a direct bandgap of 0.079 eV in comparison with the experimental bandgap of 0.18 eV [10,15,18,19,22]. It is a well-known fact that the difference in the theoretical estimates of the bandgap and its experimental value is typical because of the approximations used in the calculations [25,26]. DFT− generalized gradient approximation (GGA) gives underestimation of bandgap up to 40−60%. Such underestimation of the bandgap by GGA is because of the existence of a discontinuity in derivative of energy with respect to number of electrons [27]. Hence the experimental bandgap of around 0.18 eV is estimated as 0.079 eV. This gap appears between the light-hole valence and conduction band at Γ point in the Brillouin zone of the supercell which corresponds to L point of the primitive cell (Fig. 1a). The heavy-hole band (occurring at Σ point in the primitive cell) appeared on either side of light-hole band at Γ+δ in Γ→R direction and Γ-δ′ in M→Γ direction due to folding of the Brillouin zone in the supercell. The energy offset between the light-hole and heavy-hole valence sub-bands (ΔE) thus being 0.276 eV (between Γ and Γ+δ) and 0.263 eV (between Γ and Γ- δ′), respectively. In the electronic structure of $Sn_{31}InTe_{32}$, we see a resonance level formed because of *In* states and a decrease in energy difference between light-hole and heavy-hole valence bands with ΔE being 0.143 eV and 0.106 eV between Γ and Γ+δ and Γ- δ′, respectively (Fig. S1). Although the ideal resonant dopant *In* introduces resonance states and causes valence bands to converge, *Zn* is found to do much more than that. If we observe the electronic structure of $Sn_{31}ZnTe_{32}$ we see that introduction of *Zn* in *Sn* site leads to the appearance of resonance level in the form of split-off band 0.08 eV above the valence band touching the conduction band at Γ point. The *Zn* 's' orbital is found to contribute majorly at the Fermi level leading to appearance of a hump in the density of states (DOS) plot (Fig. 1b). *Zn* is also able to raise the heavy-hole valence band above the light-hole band by 0.12 eV and 0.11 eV at Γ+δ in Γ→R direction and Γ-δ′ in M→Γ direction, respectively, thus making the heavy-hole band contribute at room temperature. Such a feature was previously seen in the case of *Mg-In* codoped $Sn_{1-x}Pb_xTe$ which led the material exhibiting a record high Seebeck coefficient at room temperature [28]. In accordance with the previous reports, *Mg-In* codoped in SnTe introduces resonance levels and causes valence band convergence (ΔE = 0.161 eV) but it does

not raise the heavy-hole band above the light-hole band [22]. *Mg*-doped $Sn_{1-x}Pb_xTe$ and *In*-doped $Sn_{1-x}Pb_xTe$ is also devoid of such an interesting feature [28,29]. This feature appears only in the presence of *Pb*-alloyed SnTe doped with *Mg-In* [28]. This fact ascertains that *Zn* can be a more promising dopant with respect to improving the TE properties of SnTe as it eliminates the use of multiple dopants and toxic dopants.

In the electronic structure of $Sn_{16}Te_{16}$, we see that the bandgap of 0.079 eV appears at Z point and the heavy-hole band appears at M+δ in M→Γ direction 0.263 eV (ΔE) below the light-hole band with the values indicating that change in size of the supercell does not affect the energy differences between the bands of pristine SnTe (Fig. 2a). The valence band and conduction band of $Sn_{16}Te_{16}$ is seen to comprise *Te* 'p' and *Sn* 'p' states, respectively (Fig. 2b). $Sn_{15}InTe_{16}$ reveals a ΔE of 0.235 eV between Z and M+δ in M→Γ direction and 0.182 eV at R+δ′ in R→A direction (Fig. S2).

$Sn_{15}ZnTe_{16}$ exhibits a unique electronic structure with a gap of 0.093 eV at Z point and ΔE being 0.087 eV with heavy-hole band at M+δ in M→Γ direction, and the resonant state being above the light-hole valence band (ΔE = −0.144 eV between Z and A+δ in A→Z direction) in Z-R-A-Z region of Brillouin zone (Fig. 2c). We see that the projected density of states (pDOS) of $Sn_{15}ZnTe_{16}$ reveals hybridization of *Zn* 's' and *Te* 'p' orbitals to form deep-defect states near the Fermi level whereas hyper deep defect states around -4.5 eV below the Fermi level (Fig. 2d). The electronic structures and DOS of $Sn_{14}Zn_2Te_{16}$ show that further increase in concentration of *Zn* increases the gap at Z point to about ~0.2 eV with the appearance of two resonance levels with heavy-hole band at A+δ in A→Z direction moving further higher (Fig. S3). The increase in the bandgap values at Z point with increase in concentration of *Zn* and escalation of heavy-hole valence band above light-hole band predicts possible increase in 'S' values throughout the temperature range.

The transport properties of $Sn_{15}ZnTe_{16}$ were studied using BoltzTraP code (refer supplementary methods section for details) within a rigid band approximation as a function of chemical potential (μ) and temperature in the range of 300−800 K (Fig. 3). The p-type hole doping corresponds to negative 'μ' whereas the n-type electron doping corresponds to positive 'μ'. We see that the electrical conductivity values do not show a large variation with respect to temperature similar to the case of DOS (Fig. S4). The Seebeck, power factor, and thermal conductivity values are found to increase with increase in temperature at any given 'μ'. The peak power factors are found closer to 'μ' of 1 indicating that higher amount of doping would lead to enhanced ZT values. The above results warrant use of a synthetic technique which would lead to higher solubility of the dopant *Zn* to introduce all its beneficial effects.

We use a straightforward, swift, and scalable method for the preparation of *Zn*-doped SnTe via SHS process [30]. Self-compensation by means of addition of excess *Sn* is carried out to decrease the *Sn* vacancies and bring down the carrier concentration 'N_p' of pristine SnTe from 4.6×10^{20} cm^{-3} to 2.2×10^{20} cm^{-3} in self-compensated $Sn_{1.04}Te$ [22]. The non-equilibrium process of SHS helps in overcoming the solubility limit set by the equilibrium phase diagram which generally impedes the conventional synthesis [30]. Because the energy offset of valence bands in SnTe is higher than that of PbTe, to achieve the same amount of convergence by doping, higher dopant concentration is essential to obtain better Seebeck values [22]. Thus, the above process helps in achieving the desired amount of *Zn* doping (x = 0.08 mol %) without the formation of precipitates in the parent SnTe matrix. Beyond x = 0.08 mol % impurity phase started appearing in the X-ray powder diffraction (XRD). We carried out DCS on the samples to densify it, allowing us to achieve a theoretical density of 98.5%.

The XRD patterns of $Sn_{1.04-x}Zn_xTe$, where 'x' ranges from 0.02 to 0.08 mol % with Δ 0.02 mol % was indexed to NaCl structure with
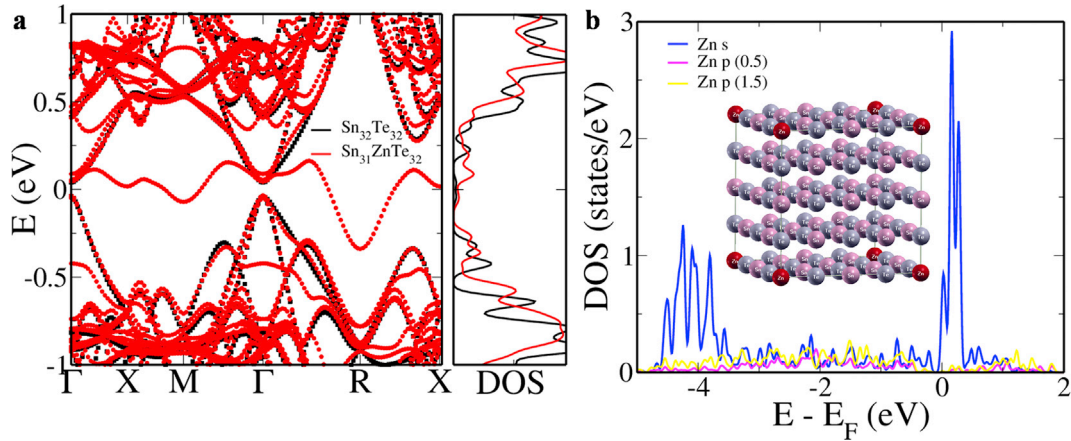
Fig. 1. a) Electronic structure of $Sn_{32}Te_{32}$ and $Sn_{31}ZnTe_{32}$; (b) contribution of *Zn* orbitals to the total DOS. Inset shows the crystal structure of $Sn_{31}ZnTe_{32}$ supercell. The light-hole valence band occurring at L point folds onto Γ point and the heavy-hole valence band occurring at Σ point folds on the Γ+δ point along Γ→R direction and Γ-δ′ along M→Γ direction. The resonant states of *Zn* can be clearly identified in the form of hump in the DOS of $Sn_{31}ZnTe_{32}$. The energies are shifted with respect to the valence band maximum of $Sn_{32}Te_{32}$, and the Fermi level of $Sn_{32}Te_{32}$ is set to zero.
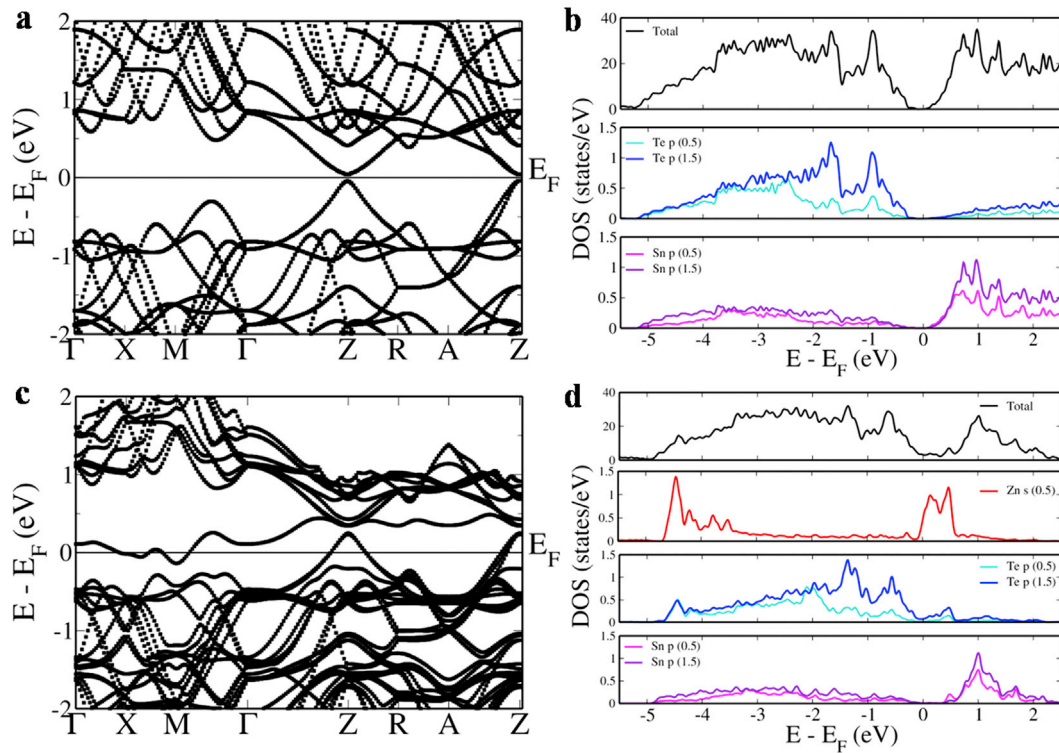

Fig. 2. Electronic structure and pDOS of $Sn_{16}Te_{16}$ (a and b); $Sn_{15}ZnTe_{16}$ (c and d).

Fm3m space group (Fig. 4a). We observe a decrease in the lattice parameter of $Sn_{1.04-x}Zn_xTe$ with increase in 'x' as the ionic radius of Zn^{2+} is smaller than Sn^{2+} (Fig. 4a inset). The agreement of lattice parameter with the Vegard's law and appearance of the single phase with lack of impurity peaks in XRD pattern points towards successful doping of *Zn* in *Sn* site. As predicted by DFT, the bandgap of the materials also increase almost linearly with increase in the dopant concentration up to 0.43 eV for x = 0.08 (Fig. S5). The difference in the values of theoretically estimated and experimentally observed bandgaps is because of the typical underestimation in DFT-based calculations as explained previously [27].

We see that at lower temperature, the 'S' values of $Sn_{1.04}Te$ is lower than pristine SnTe, but the trend gets reversed at higher

temperatures. The increase in temperature and 'x' in $Sn_{1.04-x}Zn_xTe$ is seen to bring about an increase in 'S' (Fig. 4b). A record high room temperature (300 K) 'S' of ~127 μVK^{-1} is obtained for $Sn_{0.96}Zn_{0.08}Te$. This is because of the introduction of resonance states by *Zn* as revealed by DFT studies. In addition, the increase in energy of heavy-hole valence band than light-hole band upon *Zn* doping leads to heavy-hole valence band contributing to valley degeneracy of 12 to the existing valley degeneracy of 4 of the light-hole band at room temperature itself. In general, the valence band convergence is prominent with increase in dopant concentration and temperature; and hence, at higher temperatures we see appreciable increase in the 'S' values. The raising of heavy-hole band above the light-hole band is observed in *Se*-doped PbTe around ~900 K
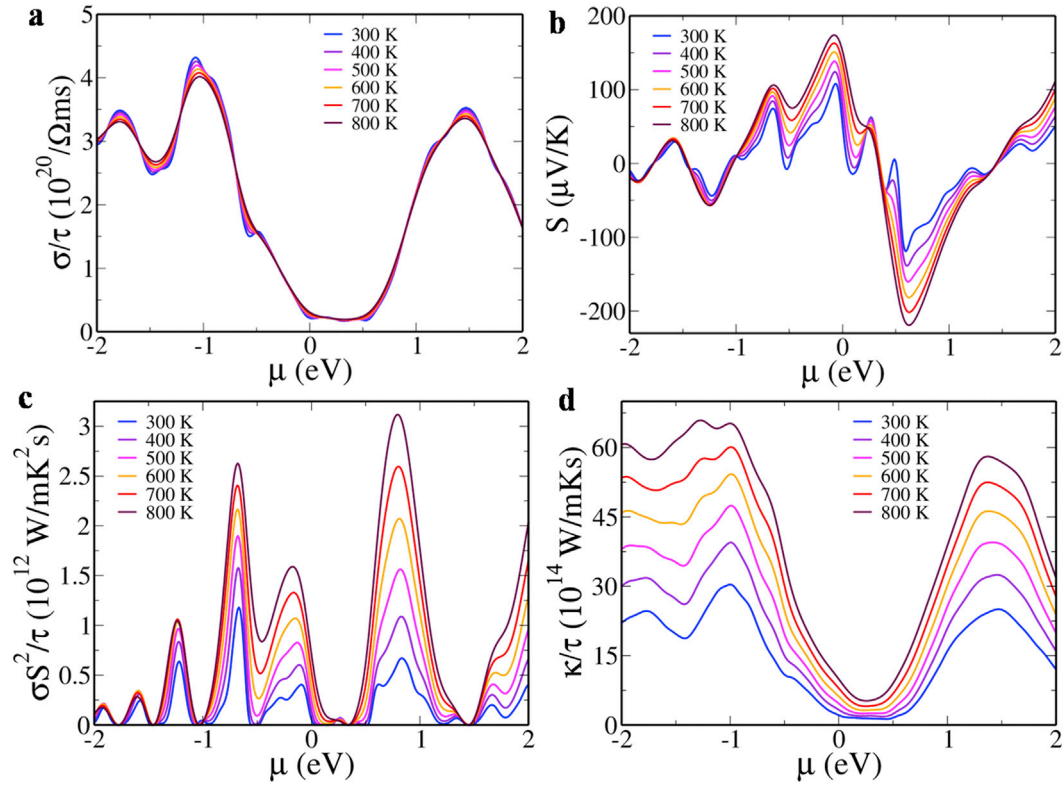
Fig. 3. a) Electrical conductivity; (b) Seebeck coefficient; (c) power factor, and (d) thermal conductivity of $Sn_{15}ZnTe_{16}$ as a function of chemical potential (μ) at various temperatures.
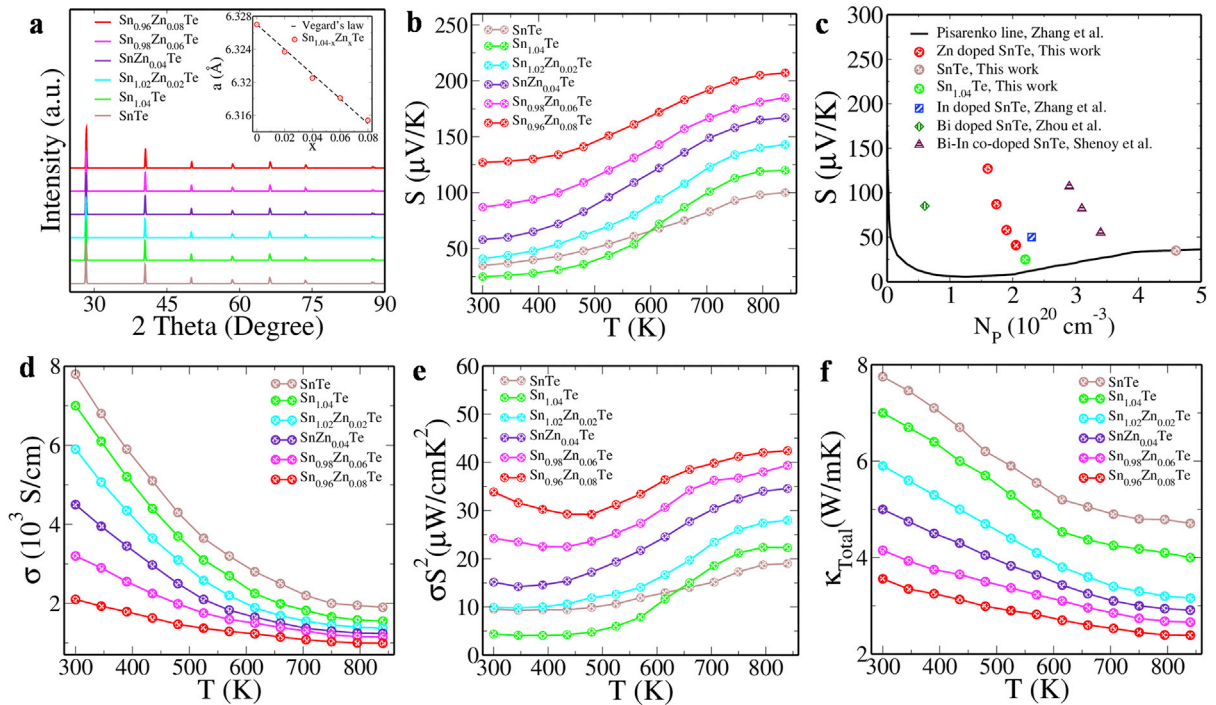

Fig. 4. a) XRD pattern of SnTe and $Sn_{1.04-x}Zn_xTe$ (inset shows lattice parameter as a function of doping concentration 'x'); (b) 'S' values of SnTe and $Sn_{1.04-x}Zn_xTe$ as a function of temperature; (c) room temperature 'S' as a function of carrier concentration 'N_p'. The Pisarenko line is derived using two valence band model (light-hole valence band with effective mass of 0.168 m_e and heavy-hole valence band with an effective mass of 1.92 m_e) with a $\Delta E = 0.35$ eV. For comparison with room temperature, 'S' values of optimized concentration of *In*, *Bi* singly doped and *Bi-In*−codoped SnTe has been marked with respect to their carrier concentration [8−10]; (d) electrical conductivity; (e) power factor; (f) total thermal conductivity of SnTe and $Sn_{1.04-x}Zn_xTe$ as a function of temperature.

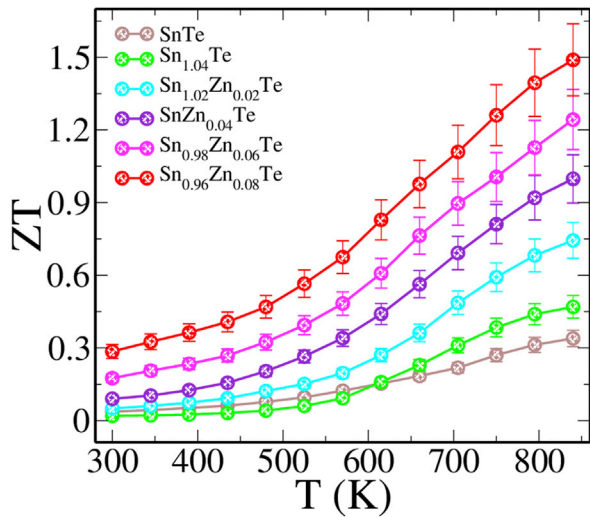**Fig. 5.** ZT of SnTe and $Sn_{1.04-x}Zn_xTe$ as a function of temperature. The ZT measurement uncertainty is about 10% (error bar).

leading to high 'S' values [31]. In the current work, because at room temperature itself we have dominant contribution of heavy-hole band, we see a large value of 'S' similar to the case of *Mg-In* codoped $Sn_{1-x}Pb_xTe$ reported earlier [28]. This is also confirmed when we compare the room temperature 'S' values with the Pisarenko plot (Fig. 4c). The 'S' value falls exactly on the line for SnTe, slightly higher for $Sn_{1.04}Te$ whereas for the *Zn*-doped samples, it is way above the predicted line. We observe the degenerating semiconducting nature of $Sn_{1.04-x}Zn_xTe$ in the electrical conductivity plot wherein the 'σ' values decrease with increase in temperature and 'x' as the carrier concentrations 'N_p' decreases from 2.2×10^{20} cm^{-3} for x = 0.00 to 1.6×10^{20} cm^{-3} for x = 0.08 (Fig. 4d). Resonant dopant such as *In* is known to enhance the 'S' values at low temperature but at higher temperatures, its performance is comparatively poor [8]. Hence, it is usually codoped with an element which can improve the performance at higher temperatures [18–20,22,23]. It is noteworthy that *Zn* by means of introducing resonance states is able to realize high performance throughout the temperature range, and hence it eliminates the requirement of a codopant.

As a consequence of high 'S' values at higher doping concentrations, we see an increase in the power factor of $Sn_{0.96}Zn_{0.08}Te$ from ~34 μWcm^{-1}K^{-2} at 300 K to ~42 μWcm^{-1}K^{-2} at 840 K in spite of decrease in 'σ' values as a function of temperature (Fig. 4e). Such a high power factor is comparable with that of *Mg-In*codoped SnTe (~42 μWcm^{-1}K^{-2} at 840 K) with a peak ZT of ~1.5 and *Ca-In* codoped SnTe (~47 μWcm^{-1}K^{-2} at 840 K) with a peak ZT of ~1.65 and much higher than *Mn-Cu-Ge* multidoped SnTe (~19 μWcm^{-1}K^{-2} at 900 K) with a record ZT peak of ~1.8 [17,19,22]. The power factor is also high compared with that of *Sr-In* codoped SnTe (~33.88 μWcm^{-1}K^{-2} at 823 K) and *Bi-In* codoped SnTe (~36 μWcm^{-1}K^{-2} at 840 K) [10,23]. Thus, the current strategy proves to be a fascinating one to improve the power factor of SnTe-based material by an addition of a single dopant.

We know that the total thermal conductivity is the sum of electronic, lattice, and bipolar thermal conductivity. We see that the total thermal conductivity of $Sn_{1.04-x}Zn_xTe$ decreases because of decrease in the electronic part of thermal conductivity as 'σ' values decrease with temperature and 'x' (Fig. 4f). In addition, the lattice part of thermal conductivity is seen to decrease because of atomic point defects introduced by the substitution of *Sn* by *Zn* (Fig. S6). These defects effectively scatter the phonons and hence, further decrease the total thermal conductivity. Bipolar thermal conduction is observed at higher temperatures as a consequence of the thermal transport by the carriers across the bandgap when the bandgap is very small. Because lattice thermal conductivity was determined by subtracting electronic component from the total thermal conductivity, the bipolar component gets added to the lattice part at higher temperatures [32,33]. The hump in the lattice thermal conductivity values of SnTe and $Sn_{1.04}Te$ beyond ~600 K is because of the bipolar contribution due to low bandgap of the material (0.18 eV) [15]. We do not see the contribution from the bipolar component to the thermal conductivity of doped samples as the bandgap of the material is increased as a result of *Zn* doping as revealed by DFT studies and experimental bandgap measurements [32,33]. The lattice thermal conductivity of 1 W/mK for $Sn_{0.96}Zn_{0.08}Te$ at 840 K high above the theoretical limit warrants further work could be done to decrease the value by other means such as introduction of defects, nanoprecipitates, mesostructuring, or strain engineering [34,35].

The synergistic effect of all the above makes $Sn_{0.96}Zn_{0.08}Te$ exhibit a record high room temperature ZT value of ~0.28 at 300 K against previous record of ~0.25 set by *Bi-In* codoped SnTe (Fig. 5)

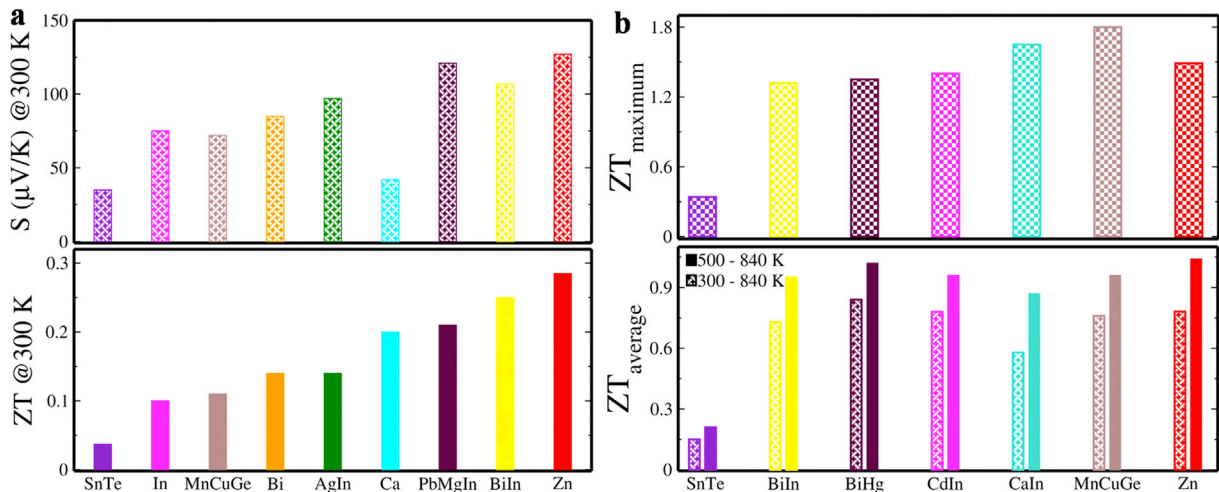**Fig. 6.** Comparison of (a) S and ZT at 300 K of $Sn_{0.96}Zn_{0.08}Te$ with reported room temperature high performing SnTe-based materials [8–10,12,17,18,28]; (b) ZT_{max} and ZT_{avg} of $Sn_{0.96}Zn_{0.08}Te$ with reported high performing SnTe-based materials [10,14,17,19,20].

[10]. We also compare the 'S' values and ZT at 300 K of SnTe-based materials which have been reported for better room temperature performances (Fig. 6a) [8−10,12,17,18,28]. Zn-doped SnTe is seen to exhibit higher 'S' values in comparison with the singly doped, codoped, or multidoped SnTe materials and hence higher ZT, which can be further improved potentially, if the thermal conductivity part is effectively tuned. $Sn_{0.96}Zn_{0.08}Te$ also gives us a decent peak ZT of ~1.49 at 840 K which is compared with the recent high-performance SnTe-based materials (Fig. 6b) [10,14,17,19,20]. Our material seems to perform better than the ones reported and has an advantage of being free from toxic elements such as Pb, Cd, and Hg [14,20,28]. Although the peak ZT of $Sn_{0.96}Zn_{0.08}Te$ is below the record high value of ~1.8 at 900 K (Mn-Cu-Ge multidoped SnTe) for SnTe-based materials, Zn-doped SnTe has higher $ZT_{average}$ of ~0.78 between 300 K and 840 K than ~0.76 (Mn−Cu−Ge multidoped SnTe) and record high value of ~1.04 between 500 and 840 K against the previous record of ~1.02 (Bi-Hg−doped SnTe) [14,17]. Because efficiency depends on $ZT_{average}$ than peak ZT for commercial applications, Zn-doped SnTe acts as a promising material for TE applications.

3. Conclusions

In the current work, we introduce for the first time, a third resonant dopant for SnTe family viz. Zn. Zn acts as a versatile dopant which engineers the electronic structure of SnTe by introducing resonant states, increasing the bandgap of SnTe, raising the heavy-hole valence band above the light-hole valence band, thereby eliminating the need to use multiple dopants. The multifaceted effects introduced by Zn in SnTe leads to both record high room temperature Seebeck value (~127 μVK^{-1} at 300 K) and ZT (~0.28 at 300 K). A peak ZT of ~1.49 at 840 K and a record high $ZT_{average}$ value of ~1.04 between 500 and 840 K is also exhibited by the material. This work with a combination of theory and experiments establishes Zn-doped SnTe as a promising candidate for TE applications.

Conflicts of interest

There are no conflicts of interest to declare.

Acknowledgements

Appendix A. Supplementary data

Supplementary data to this article can be found online at https://doi.org/10.1016/j.mtphys.2019.100158.

References

[1] G.J. Snyder, E.S. Toberer, Complex thermoelectric materials, Nat. Mater 7 (2008) 105−114.
[2] F. Guo, B. Cui, H. Geng, Y. Zhang, H. Wu, Q. Zhang, B. Yu, S.J. Pennycook, W. Cai, J. Sui, Simultaneous boost of power factor and figure of merit in in-Cu Co-doped SnTe, Small 15 (2019) 1902493.
[3] R. Moshwan, X.L. Shi, W.D. Liu, Y. Wang, S. Xu, J. Zou, Z.G. Chen, Enhancing thermoelectric properties of InTe nanoprecipitates embedded $Sn_{1-x}In_xTe$ microcrystals through anharmonicity and strain engineering, ACS, Appl. Energy Mater 2 (2019) 2965−2971.
[4] S. Hao, V.P. Dravid, M.G. Kanatzidis, C. Wolverton, Computational strategies for design and discovery of nanostructured thermoelectrics, npj Computational Materials 5 (2019) 58.
[5] G. Tan, L.D. Zhao, M.G. Kanatzidis, Rationally designing high-performance bulk thermoelectric materials, Chem. Rev. 116 (2016) 12123−12149.
[6] R. Moshwan, L. Yang, J. Zou, Z.G. Chen, Eco-friendly SnTe thermoelectric materials: progress and future challenges, Adv. Funct. Mater. 27 (2017) 1703278.
[7] S. Li, X. Li, Z. Ren, Q. Zhang, Recent progress towards high performance of tin chalcogenide thermoelectric materials, J. Mater. Chem. A 6 (2018) 2432−2448.
[8] Q. Zhang, B. Liao, Y. Lan, K. Lucas, W. Liu, K. Esfarjani, C. Opeil, D. Broido, G. Chen, Z. Ren, High thermoelectric performance by resonant dopant Indium in nanostructured SnTe, Proc. Natl. Acad. Sci. U. S. A 110 (2013) 13261−13266.
[9] Z. Zhou, J. Yang, Q. Jiang, Y. Luo, D. Zhang, Y. Ren, X. He, J. Xin, Multiple effects of Bi doping in enhancing the thermoelectric properties of SnTe, J. Mater. Chem. A 4 (2016) 13171−13175.
[10] S.U. Shenoy, D.K. Bhat, Electronic structure engineering of tin telluride through Co-doping of bismuth and Indium for high performance thermoelectrics: a synergistic effect leading to record high room temperature ZT in tin telluride, J. Mater. Chem. C 7 (2019) 4817−4821.
[11] L. Zhao, J. Wang, J. Li, J. Liu, C. Wang, J. Wang, X. Wang, High thermoelectric performance of Ag doped SnTe polycrystalline bulks via the synergistic manipulation of electrical and thermal transport, Phys. Chem. Chem. Phys. 21 (2019) 17978−17984.
[12] R.A.R.A. Orabi, N.A. Mecholsky, J. Hwang, W. Kim, J.S. Rhyee, D. Wee, M. Fornari, Band degeneracy, low thermal conductivity, and high thermoelectric figure of merit in SnTe-CaTe alloys, Chem. Mater. 28 (2016) 376−384.
[13] J. Tang, B. Gao, S. Lin, X. Wang, X. Zhang, F. Xiong, W. Li, Y. Chen, Y. Pei, Manipulation of solubility and interstitial defects for improving thermoelectric SnTe alloys, ACS Energy Lett. 3 (2018) 1969−1974.
[14] G. Tan, F. Shi, J.W. Doak, H. Sun, L.D. Zhao, P. Wang, C. Uher, C. Wolverton, V.P. Dravid, M.G. Kanatzidis, Extraordinary role of Hg in enhancing the thermoelectric performance of p-type SnTe, Energy Environ. Sci. 8 (2015) 267−277.
[15] A. Banik, U.S. Shenoy, S. Anand, U.V. Waghmare, K. Biswas, Mg alloying in SnTe facilitates valence band convergence and optimizes thermoelectric properties, Chem. Mater. 27 (2015) 581−587.
[16] F. Guo, B. Cui, Y. Liu, X. Meng, J. Cao, Y. Zhang, R. He, W. Liu, H. Wu, S.J. Pennycook, W. Cai, J. Sui, Thermoelectric SnTe with band convergence, dense dislocations, and interstitials through Sn self-compensation and Mn alloying, Small 14 (2018) 1802615.
[17] J. Tang, B. Gao, S. Lin, J. Li, Z. Chen, F. Xiong, W. Li, Y. Chen, Y. Pei, Manipulation of band structure and interstitial defects for improving thermoelectric SnTe, Adv. Funct. Mater. 28 (2018) 1803586.
[18] A. Banik, U.S. Shenoy, S. Saha, U.V. Waghmare, K. Biswas, High power factor and enhanced thermoelectric performance of SnTe-$AgInTe_2$: synergistic effect of resonance level and valence band convergence, J. Am. Chem. Soc. 138 (2016) 13068−13075.
[19] D.K. Bhat, S.U. Shenoy, Enhanced thermoelectric performance of bulk tin telluride: synergistic effect of calcium and Indium Co-doping, Mat. Today Phys. 4 (2018) 12−18.
[20] G. Tan, F. Shi, S. Hao, H. Chi, L.D. Zhao, C. Uher, C. Wolverton, V.P. Dravid, M.G. Kanatzidis, Codoping in SnTe: enhancement of thermoelectric performance through synergy of resonance levels and band convergence, J. Am. Chem. Soc. 137 (2015) 5100−5112.
[21] H. Wang, J. Hwang, C. Zhang, T. Wang, W. Su, H. Kim, J. Kim, J. Zhai, X. Wang, H. Park, W. Kim, C. Wang, Enhancement of the thermoelectric performances of bulk SnTe alloys via the synergistic effect of band structure modification and chemical bond softening, J. Mater. Chem. A 5 (2017) 14165−14173.
[22] D.K. Bhat, S.U. Shenoy, High thermoelectric performance of Co-doped tin telluride due to synergistic effect of magnesium and Indium, J. Phys. Chem. C 121 (2017) 7123−7130.
[23] R. Moshwan, W.D. Liu, X.L. Shi, Y.P. Wang, J. Zou, Z.G. Chen, Realizing high thermoelectric properties of SnTe via synergistic band engineering and structure engineering, Nano Energy 65 (2019) 104056.
[24] S.K. Kihoi, H. Kim, H. Jeong, H. Kim, J. Ryu, S. Yi, H.S. Lee, Thermoelectric properties of Mn, Bi and Sb Co-doped SnTe with a low lattice thermal conductivity, J. Alloy. Comp. 806 (2019) 361−369.
[25] H. Bantawal, M. Sethi, S.U. Shenoy, D.K. Bhat, Porous graphene wrapped $SrTiO_3$ nanocomposite: Sr-C bond as an effective coadjutant for high performance photocatalytic degradation of methylene blue, ACS Appl. Nano Mater 2 (2019) 6629−6636.
[26] H. Bantawal, S.U. Shenoy, D.K. Bhat, Band engineering of SrTiO3: effect of synthetic technique and site occupancy of doped rhodium, J. Phys. Chem. C 122 (2018) 27567−27574.
[27] J.P. Perdew, Density functional theory and the band gap problem, Int. J. Quantum Chem. 28 (1985) 497−523.
[28] S. Roychowdhury, U.S. Shenoy, U.V. Waghmare, K. Biswas, An enhanced Seebeck coefficient and high thermoelectric performance in p-type in and Mg co-doped $Sn_{1-x}Pb_xTe$ via the Co-adjuvant effect of the resonance level and heavy hole valence band, J. Mater. Chem. C 5 (2017) 5737−5748.
[29] S. Shenoy, D.K. Bhat, Enhanced bulk thermoelectric performance of $Pb_{0.6}Sn_{0.4}Te$: effect of magnesium doping, J. Phys. Chem. C 121 (2017) 20696−20703.

[30] T. Liang, X. Su, X. Tan, G. Zheng, X. She, Y. Yan, X. Tang, C. Uher, Ultra-fast non-equilibrium synthesis and phase segregation in $In_xSn_{1-x}Te$ thermoelectrics by SHS-PAS processing, J. Mater. Chem. C 3 (2015) 8550−8558.

[31] Y. Pei, X. Shi, A. Lalonde, H. Wang, L. Chen, G.J. Snyder, Convergence of electronic bands for high performance bulk thermoelectrics, Nature 473 (2011) 66−69.

[32] S. Roychowdhury, U.S. Shenoy, U.V. Waghmare, K. Biswas, Tailoring of electronic structure and thermoelectric properties of a topological crystalline Insulator by chemical doping, Angew. Chem. Int. Ed. 54 (2015) 15241−15245.

[33] S. Roychowdhury, U.S. Shenoy, U.V. Waghmare, K. Biswas, Effect of potassium doping on electronic structure and thermoelectric properties of topological crystalline Insulator, Appl. Phys. Lett. 108 (2016) 193901.

[34] J. Tang, Z. Yao, Z. Chen, S. Lin, X. Zhang, F. Xiong, W. Li, Y. Chen, Y. Pei, Maximization of transporting bands for high-performance SnTe alloy thermoelectrics, Mat. Today Phys. 9 (2019) 100091.

[35] Y. Wu, Z. Chen, P. Nan, F. Xiong, S. Lin, X. Zhang, Y. Chen, L. Chen, B. Ge, Y. Pei, Lattice strain advances thermoelectrics, Joule 3 (2019) 1−13.